A NEW THEORETICAL MODEL FOR GUIDING THE GAS EXTRACTION IN COAL MINES

by

Jing XIE[a], Zetian ZHANG[a*], Mingzhong GAO[a], Ru ZHANG[a], Man WANG[b], Wencheng JIN[c], and Yi LUO[c]

[a] State Key Laboratory of Hydraulics and Mountain River Engineering,
College of Water Resource and Hydropower, Sichuan University, Chengdu, China
[b] China Pingmei Shenma Energy and Chemical Industry Group Co., LTD, Pingdingshan, China
[c] School of Architecture and Environment, Sichuan University, Chengdu, China

Original scientific paper
https://doi.org/10.2298/TSCI17S1293X

Based on the fractal-percolation properties, the equivalent permeability analysis of 3-D discrete fracture network models are investigated and analyzed for the first time. The 3-D fractal dimension was calculated with the 3-D fracture density, the mean major axis of fracture and the aspect ratio of major to minor axis. The reconstructed mining-induced fracture network model was used to validate that the correlation between the predicted and actual results is very strong in a sense. The equivalent permeability results can be adopted to guide the gas extraction in coal mines.

Key words: *gas extraction, 3-D discrete fracture network , fracture density, percolation-fractal properties, equivalent permeability analysis*

Introduction

The method of discrete fracture network (DFN) generation is one of the basic approaches proposed to model the transport properties in fracture reservoirs. An accurate estimation of the fracture network permeability is an important and crucial task. However, it is still a challenge to conduct fluid flow prediction even though numbers of extensive works were carried out on characterizing fractured rocks over the last years [1]. By means of relating the fracture network properties to fluid flow process, it may be an effective way to achieve the permeability estimation.

As for the reconstructed DFN model, the geometrical parameters, such as the fracture length, size, shape, density, aperture and orientation, are the fundamental data of DFN modeling. For example, the hypothesis that fractures are parallel to each other with the planar shape of disks or parallelograms and generated the Poisson disc model was proposed in [2]. The 3-D DFN reconstruction with geometrical parameters collecting from the field borehole test was achieved in [3]. The geometrical parameters for controlling the fracture network permeability were reported in [4]. The hydraulic properties of fractured rock mass, when distributed fracture aperture was correlated with fracture trace length, were studied in [5]. With the increasing of fracture length and density, the connectivity of fracture network increases [6]. The fracture permeability would reduce due to the perpendicular fractures to the direction of the flow [7].

* Corresponding author, e-mail: znthe123@126.com

Natural fracture patterns present the fractal characteristics [8]. The fractal dimension (FD) shows the tendency of an object to spread or fill in the space and to describe the complexity of fracture network, see [9] and the reference therein. The percolation theory also is a powerful concept for analyzing the transport properties of random systems [4]. The equivalent permeability of 2-D fracture network can be strongly correlated to different impact parameters [10]. In the 3-D case, the fracture network properties were considered. For example, the 3-D model containing the 2-D fracture planes with power-law size distribution uniformly located in the space was studied in [11]. The percolation threshold and permeability of anisotropic 3-D fracture network was suggested in [12]. In order to handle the real-world engineering problems in mining rocks, it is necessary to develop a practical and easy technique to estimate the anisotropic fractal-percolation properties of the 3-D DFN model. Owing to motivation by the previous results, the main aims of this manuscript is to study the fractal-percolation properties and to establish the 3-D DFN model for mining fracture network reconstructed to conduct the equivalent permeability analysis.

The FD and Percolation theory

The fractal theory developed by Mandelbrot [13] is usually considered as one important method to describe different synthetic and natural fractal objects. Box counting is the traditional and typical method to measure FD of fractures [10]. The 2-D measuring window (MW) can be with different orientation. A series of square-boxes ($r \times r$) or cube-boxes ($r \times r \times r$) are used to cover the fractures in measured window (MW) or measured cube (MC). The number of square-boxes or cube-boxes accords the following relationship [14]:

$$N(r) \propto r^{-D} \tag{1}$$

where $N(r)$ is the number of square-boxes or cube-boxes covering the fractures, r – the square or box size, and D is the value of FD.

A practical and general mathematical way to describe its connectivity, conductivity, and permeability was considered in [15]. Assuming that some sites or bonds are open to flow with a probability, p, a smaller p means a smaller connected occupied site (called an isolated cluster), and a higher p means a bigger connected occupied site. As the probability increasing to a particular value known as the percolation threshold, p_c, the connected occupied sites will connect two opposite boundaries together, see, *e. g.*, [4]. There exists a simple analytical term known as power law [16]:

$$P(p) \propto (p - p_c)^{\mu} \quad p > p_c \tag{2}$$

where $P(p)$ is the probability that a bond or a site connects to the spanning cluster in the domain and μ is an exponent depending on the dimensionality of the domain not the lattice characteristics.

In the continuum percolation, some research, see, *e. g.*, [15], has assumed that there is a similar relationship between the effective permeability of a fractured matrix and percolation characteristics with eq. (2):

$$K_{\text{eff}} \propto (p - p_c)^{\mu} \tag{3}$$

where K_{eff} is the effective permeability. As displayed in fig. 1, four 2-D MW in the 3-D fracture network system are chosen to study the anisotropic characteristics based on the fractal and statistical properties. The domain normal to X, Y, and Z axis are noted as MW1, MW2, and MW3, respectively. The domain parallel to the average orientation of fractures is noted as MW4. The 2-D FD (D_{2D}) each MW is noted as the non-dimensional equation of the form:

$$D_{\text{2D-}(\perp X,\perp Y,\perp Z,//)} \propto \left(p_{(\perp X,\perp Y,\perp Z,//)} - p_c\right)^{\mu_{(\perp X,\perp Y,\perp Z,//)}} \tag{4}$$

where $D_{\text{2D-}(\perp X,\perp Y,\perp Z,//)}$ is the FD of MW with different directions, $p_{(\perp X,\perp Y,\perp Z,//)} - p_c$ is the difference between the occupancy probability with different direction and percolation threshold, and $\mu_{(\perp X,\perp Y,\perp Z,//)}$ is a universal exponent with different direction.

Generally, the excluded area of 2-D fractures can be described by the following expression [17]:

$$A_{\text{ex}} = \frac{2}{\pi} l^2 \tag{5}$$

where A_{ex} is the excluded area and l is the fracture length. This equation is applied for isotropic case. However, the fracture length in this 3-D model is not a constant. To consider the anisotropic case, the average fracture length $\bar{l}$ of each domain is used when analyzing A_{ex} of each MW.

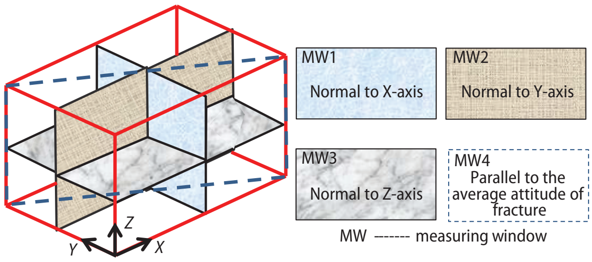

Figure 1. The different MW for fractal-percolation analysis

The 2-D fracture density ρ_{2D} of a MW is given by [12]:

$$\rho_{2D} = \frac{N_{fr}}{S} \tag{6}$$

where N_{fr} is total fracture numbers in the domain area and S is the area of the domain.

$$\rho'_{2D} = \rho_{2D} A_{\text{ex}} \tag{7}$$

Fractal properties of 3-D DFN models with different parameters

A method for the DFN generation based on the borehole monitoring can obtain orientation of fracture and the fracture number of different intersection type on borehole wall [3]. The structural homogeneity zone, the number of fracture, the volume density frequency and the 3-D probability distribution of fracture are determined by the MATLAB Toolbox RJNS^{3D} and Dips. Three parameters based on the field statistics and connect to the real fracture network are considered to evaluate the fractal properties of 3-D DFN models, including 3-D fracture density (denoted by ρ_{3D}, change from 0.005, 0.010, 0.015 to 0.020), the mean major axis of fracture (denoted by μ_a, change from 10, 15, 20 to 25) and the aspect ratio of major to minor axis (denoted by K, change from 1, 3, 5 to 7). The standard deviation σ_a, the dip direction α, and the dip angle β are 1, 135°, and 45°, respectively. Now, the square-box size is changing from 4, 2, 1, 0.5, to 0.25 m and the cube-box size is changing from 2.5, 2, 1.5, 1, to 0.5 m. From eq. (1), the fractal properties of 48 calculating patterns are displayed in fig. 2. If ρ_{3D} and μ_a are constants, and μ_a is higher, then 3-D FD (denoted by D_{3D}) is smaller, as displayed in fig. 3(a). If ρ_{3D} and K are constant (or μ_{a} and K remain stable), and μ_{a} (or ρ_{3D}) are higher, $D_{\text{3D}}$is larger, as shown in figs. 3(b) and 3(c). If K is larger, then the fractures are relatively slender. Compared between the conditions, the later shows a less advantage for the generation of the complex fracture network. In the case, the fractal relationship can be written:

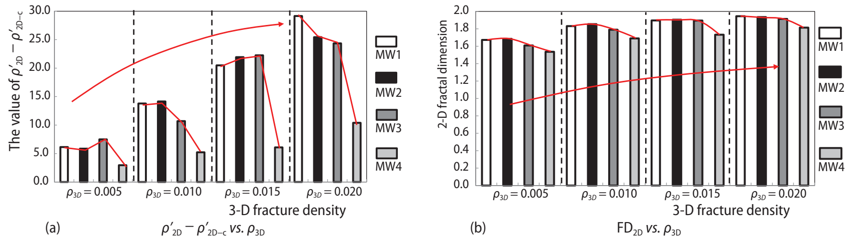

Figure 2. Anisotropic characteristics of DFN models with different MW

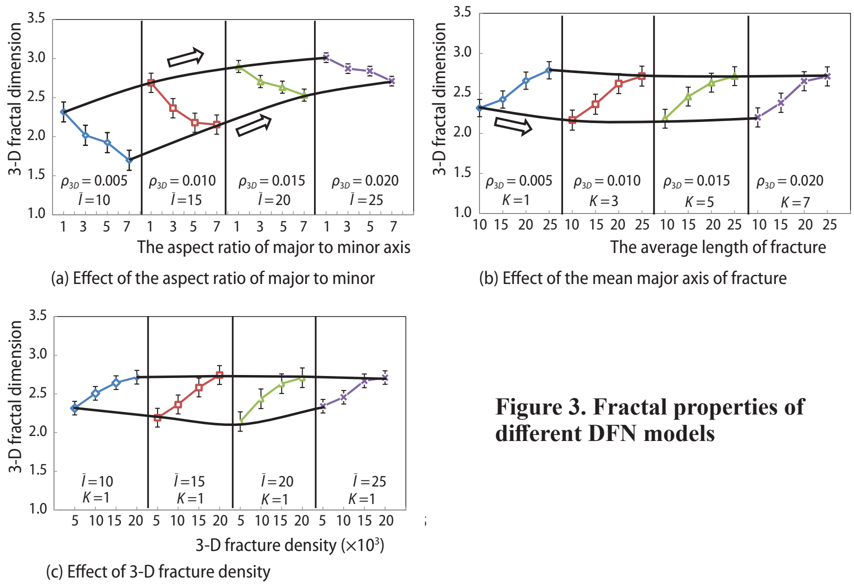

Figure 3. Fractal properties of different DFN models

$$D_{3D} \propto \rho_{3D},\ \mu_a,\ \frac{1}{K} \tag{8}$$

The anisotropic percolation: fractal properties of a 3-D DFN model

The percolation and fractal properties related with the permeability are relatively easy to get from the field statistics or DFN models. Here, eight new DFN model numbered 49 to 56 were investigated. Other parameters of 49-52 patterns are the fracture lengths in the mean major axis are, respectively, 30 for 49-52 patterns and 25 for 53-56 patterns, the standard deviation of fracture length is 1, the dip direction is 135°, the dip angle is 45°, and the aspect ratio of major to minor axis is 2. The difference between dimensionless density and dimensionless percolation threshold, denoted by $\rho'_{2D} - \rho'_{2D\text{-c}}$, islisted in tab. 1. The dimensionless percolation threshold, denoted by $\rho'_{2D\text{-c}}$, is 3.6 [4].

As presented in fig. 2, MW1, MW2, and MW3 show the differences with three principal directions of DFN models. The MW4 takes the orientation of the fractures into consideration. The 2-D FD (denoted by D_{2D}) and $\rho'_{2D} - \rho'_{2D\text{-c}}$ of MW are regarded as the evaluation index of anisotropic characteristics. With the increasing of 3-D fracture density (denoted by ρ_{3D}),

Table 1. The computational results of percolation properties for 49 to 56 patterns

No.	ρ_{3D}	ρ_{2D}	ρ'_{2D}	$\rho'_{2D}-\rho'_{2D-c}$	No.	ρ_{3D}	ρ_{2D}	ρ'_{2D}	$\rho'_{2D}-\rho'_{2D-c}$
49-MW1	0.005	0.158	9.745	6.145	53-MW1	0.005	0.121	4.803	1.203
49-MW2	0.005	0.160	9.460	5.860	53-MW2	0.005	0.137	4.870	1.270
49-MW3	0.005	0.113	11.088	7.488	53-MW3	0.005	0.104	5.843	2.243
49-MW4	0.005	0.104	6.544	2.944	53-MW4	0.005	0.066	3.346	-0.254
50-MW1	0.010	0.291	17.391	13.791	54-MW1	0.010	0.234	9.504	5.904
50-MW2	0.010	0.320	17.745	14.145	54-MW2	0.010	0.244	9.565	5.965
50-MW3	0.010	0.227	14.287	10.687	54-MW3	0.010	0.186	12.119	8.519
50-MW4	0.010	0.193	8.825	5.225	54-MW4	0.010	0.143	5.819	2.219
51-MW1	0.015	0.426	24.091	20.491	55-MW1	0.015	0.336	13.310	9.710
51-MW2	0.015	0.438	25.527	21.927	55-MW2	0.015	0.346	12.380	8.780
51-MW3	0.015	0.338	25.843	22.243	55-MW3	0.015	0.254	15.313	11.713
51-MW4	0.015	0.254	9.680	6.080	55-MW4	0.015	0.201	8.044	4.444
52-MW1	0.020	0.594	32.741	29.141	56-MW1	0.020	0.520	21.396	17.796
52-MW2	0.020	0.572	29.039	25.439	56-MW2	0.020	0.482	19.391	15.791
52-MW3	0.020	0.420	27.955	24.355	56-MW3	0.020	0.361	23.960	20.360
52-MW4	0.020	0.303	14.002	10.402	56-MW4	0.020	0.313	10.009	6.409

both D_{2D} and $\rho'_{2D}-\rho'_{2D-c}$ of each MW are increasing gradually. However, an obvious difference occurs among four MW illustrated in fig. 2(a). $\rho'_{2D}-\rho'_{2D-c}$ of MW1, MW2, and MW3 is much larger than that of MW4.

As shown in fig. 4, D_{2D} is plotted against ρ_{3D} and $\rho'_{2D}-\rho'_{2D-c}$. Due to the result [12], the equations for the different MW are presented in tab. 2. If ρ_{3D} can be determined, we can select the particular equation to evaluate the D_{2D} of MW in different directions, and present directly the feedback of the anisotropic characteristics of 3-Dreconstructed DFN models. Obviously, our method can provide a feasible approach to conduct the quantitatively analysis of the 3-D DFN.

Following the calculation of the patterns, D_{3D} is presented:

$$\begin{aligned} D_{3D} = &-0.0230\ln\left(\rho'_{2D-\perp X}-\rho'_{2D-c}\right)-0.0303\ln\left(\rho'_{2D-\perp Y}-\rho'_{2D-c}\right)\cdot \\ &\cdot 0.1254\ln\left(\rho'_{2D-\perp Z}-\rho'_{2D-c}\right)+0.0775\ln\left(\rho'_{2D-//}-\rho'_{2D-c}\right)+2.5351 \\ \text{or}\quad &0.1132\ln(\rho_{3D})-0.5178\ln\left(\rho'_{2D-\perp X}-\rho'_{2D-c}\right)+0.3116\ln\left(\rho'_{2D-\perp Y}-\rho'_{2D-c}\right)+ \\ &+0.0626\ln\left(\rho'_{2D-\perp Z}-\rho'_{2D-c}\right)+0.2465\ln\left(\rho'_{2D-//}-\rho'_{2D-c}\right)+3.3327 \end{aligned} \tag{9}$$

The structure relationship between D_{2D} and D_{3D} is given:

$$D_{3D}=16.4444D_{2D-\perp X}-2.7176D_{2D-\perp Y}-5.3141D_{2D-\perp Z}-7.1035D_{2D-//}-0.7320 \tag{10}$$

We notice that the subscripts in the eqs. (9) and (10) are the same meaning as eq. (4) referring to the orientation of the MW. The coefficients are fitted by MATLAB with the use of the least square method. From eq. (10), we may present the link of the 2-D properties to 3-D properties.

Application on the reconstructed mining-induced fracture network model in rocks

In the reconstructed mining-induced fracture network (MFN), based on the field borehole test and statistical analysis, we consider the parameters of the mining sample, such as the

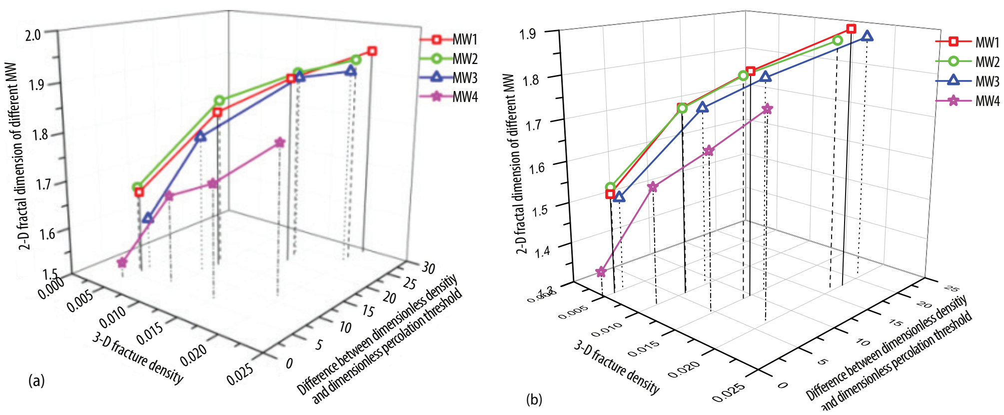

Figure 4. The difference between dimensionless density and dimensionless percolation threshold

Table 2. The equations among D_{2D}, ρ_{3D}, and $\rho'_{2D} - \rho'_{2D\text{-c}}$

Equation	R^2
$D_{2D-\perp X} = 0.0958\ln(\rho_{3D}) + 0.0879\ln(\rho'_{2D} - \rho'_{2D-c}) + 2.029$	0.9976
$D_{2D-\perp Y} = 0.0699\ln(\rho_{3D}) + 0.0971\ln(\rho'_{2D} - \rho'_{2D-c}) + 1.897$	0.9926
$D_{2D-\perp Z} = 0.1296\ln(\rho_{3D}) + 0.0908\ln(\rho'_{2D} - \rho'_{2D-c}) + 2.135$	0.9796
$D_{2D-\perp} = 0.0906\ln(\rho_{3D}) + 0.1201\ln(\rho'_{2D} - \rho'_{2D-c}) + 1.893$	0.9854
$D_{2D-\perp X} = 0.1322\ln(\rho'_{2D} - \rho'_{2D-c}) + 1.498$	0.9515
$D_{2D-\perp \mathrm{Y}} = 0.1301\ln(\rho'_{2D} - \rho'_{2D-c}) + 1.509$	0.9628
$D_{2D-\perp \mathrm{Z}} = 0.172\ln(\rho'_{2D} - \rho'_{2D-c}) + 1.358$	0.9187
$D_{2D-\perp} = 0.1846\ln(\rho'_{2D} - \rho'_{2D-c}) + 1.394$	0.8980

aspect ratio of major to minor axis, rotation angle (163°), fracture orientation (266.085°/50.175°), and 3-D fracture density (0.0378), [3]. As shown in fig. 5, the mining sample is placed in the X-direction, and Y and Z is the horizontal and vertical directions of the mining face, respectively. As shown in fig. 6, $D_{2D\text{-}\perp X}$, $D_{2D\text{-}\perp Y}$, $D_{2D\text{-}\perp Z}$, and $D_{2D\text{-}//}$ are listed in tab. 2. From eqs. (9) and (10), we obtain D_{3D}. The fitting values of D_{3D} using $\rho'_{2D} - \rho'_{2D\text{-c}}$ and ρ_{3D} is much better than others. To improve the accuracy of D_{3D}, the MW in different directions should be considered.

With the use of the large numbers of 2-D fracture network analysis, we have [4]:

$$K_{\text{eff}} = 88.411\left(\rho'_{2D} - \rho'_{2D-c}\right)^{0.4622} \qquad (R^2 = 0.8494) \tag{11}$$

where K_{eff} represents the effective fracture network permeability and R^2 is regression coefficient.

As shown in fig. 7, the MW1 is parallel to the mining face, the MW2 is parallel to the roadside, and the MW3 is parallel to the coal seam floor. The value of the MW2 is much higher than other directions when MW is parallel to the roadside. The coal rocks along the direction of roadside have a better connectivity. Gas extraction is a traditional method used for gas production. The orientation of the extracting borehole is one of the key factors to maintain the extracting efficiency and to achieve the mining safety standards. Form equivalent fracture network permeability (EFNP) calculating results based on eq. (11), the gas extracting boreholes should

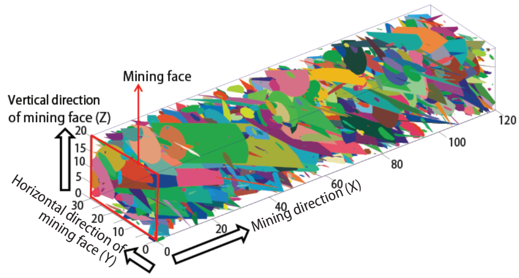

Figure 5. The reconstructed MFN model, [3]
(*for color image see journal web site*)

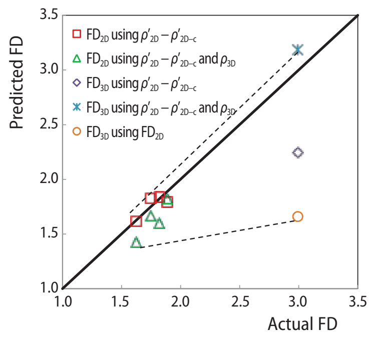

Figure 6. Predicted FD *vs.* actual FD

be deflected to the roadside as much as possible. It can be seen that the anisotropic fractal-percolation properties of the 3-D DFN model can be practically estimated through this approach.

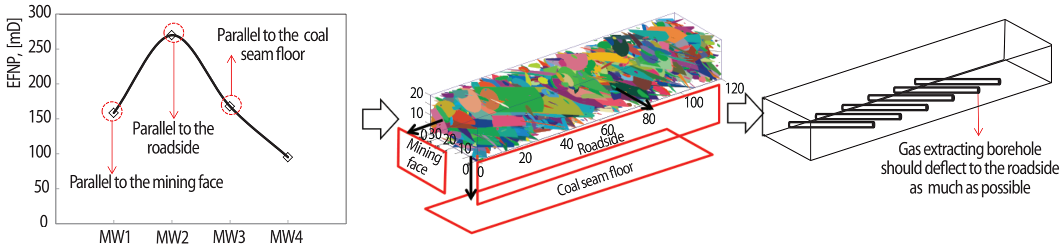

Figure 7. The EFNP results to the gas extraction in coal mines
(*for color image see journal web site*)

Conclusion

In our work, the fractal-percolation properties were investigated and an efficient application of the 3-D DFN models in mining samples was analyzed in detail. It is showed that the 3-D FD is proportional to 3-D fracture density and the mean major axis of fracture, and that it is an inverse correlation with the aspect ratio of major to minor axis. A different combination of effect parameters brings out a quite different evolution of 3-D FD. With increases of K and ρ_{3D} (or K and μ_a), the 3-D FD mostly remains obvious anisotropic characteristic. For a direct description on the equivalent permeability analysis of the 3-D DFN models, it is still an open problem.

Acknowledgment

The study was financially supported by the State Key Research Development Program of China (Grant No. 2016YFC0600701).

Nomenclature

- A_{ex} – excluded area, [m^2]
- D – FD, [–]
- D_{2D} – 2-D FD, [–]
- D_{3D} – 3-D FD, [–]
- EFNP – equivalent fracture network permeability, [mD]
- K – aspect ratio of major to minor axis, [–]
- K_{eff} – effective permeability, [m^2]
- l – fracture length, [m]
- $N(r)$ – number of square-boxes or cube-boxes, [–]
- N_{fr} – total fracture number, [–]
- p – probability, [–]
- p_c – percolation threshold, [–]

R – regression coefficient, [–]
p – probability, [–]
r – square or box size, [m]
S – area of the domain, [m^2]

Greek symbols

α – the dip direction, [°]
β – the dip angle, [°]
μ – an exponent
μ_a – mean major axis of fracture, [m]
ρ'_{2D} – dimensionless density, [–]
$\rho'_{2D\text{-}c}$ – dimensionless percolation threshold [–]
ρ_{2D} – 2-D fracture density, [m^{-2}]
ρ_{3D} – 3-D fracture density, [m^{-3}]
σ_a – standard deviation, [–]

References

[1] Berkowitz, B., Analysis of Fracture Network Connectivity Using Percolation Theory, *Mathematical Geology*, *27* (1995), 4, pp. 467-483
[2] Warburton, P., A Stereological Interpretation of Joint Trace Data, *International Journal of Rock Mechanics and Mining Sciences & Geomechanics Abstracts*, *17* (1980), 4, pp. 181-190
[3] Jin, W., *et al.*, Elliptical Fracture Network Modeling with Validation in Datong Mine, China, *Environmental Earth Sciences*, *73* (2015), 11, pp. 7089-7101
[4] Jafari, A., Babadagli, T., Relationship between Percolation-Fractal Properties and Permeability of 2-D Fracture Networks, *International Journal of Rock Mechanics and Mining Sciences*, *60* (2013), 6, pp. 353-362
[5] Baghbanan, A., Jing, L., Hydraulic Properties of Fractured Rock Masses with Correlated Fracture Length and Aperture, *International Journal of Rock Mechanics and Mining Sciences*, *44* (2007), 5, pp. 704-719
[6] Rossen, W., *et al.*, Connectivity and Permeability in Fracture Networks Obeying Power-Law Statistics, *Proceedings*, Society of Petroleum Engineers, SPE Permian Basin Oil and Gas Recovery Conference, Midland, Tex., USA, Vol. 50, 2000, pp. 2226-2232
[7] Babadagli, T., Fractal Analysis of 2-D Fracture Networks of Geothermal Reservoirs in South-Western Turkey, *Journal of Volcanology and Geothermal Research*, *112* (2001), 1, pp. 83-103
[8] La Pointe, P., A Method to Characterize Fracture Density and Connectivity through Fractal Geometry, *International Journal of Rock Mechanics and Mining Sciences & Geomechanics Abstracts*, *25* (1988), 6, pp. 421-429
[9] Berkowitz, B., Hadad, A., Fractal and Multifractal Measures of Natural and Synthetic Fracture Networks, *Journal of Geophysical Research: Solid Earth*, *1021* (1997), 6, pp. 12205-12218
[10] Jafari, A., Babadagli, T., Estimation of Equivalent Fracture Network Permeability Using Fractal and Statistical Network Properties, *Journal of Petroleum Science and Engineering*, *92* (2012), 4, pp. 110-123
[11] Mourzenko, V., *et al.*, Macroscopic Permeability of Three-Dimensional Fracture Networks with Power-Law Size Distribution, *Physical Review E*, *69* (2004), 6, 066307
[12] Khamforoush, M., *et al.*, Permeability and Percolation of Anisotropic Three-Dimensional Fracture Networks, *Physical Review E*, *77* (2008), 5, 056307
[13] Mandelbrot, B., B., Stochastic Models for the Earth's Relief, the Shape and the Fractal Dimension of the Coastlines, and the Number-Area Rule for Islands, *Proceedings of the National Academy of Sciences of the United States*, *72* (1975), 10, pp. 3825-3828
[14] Barton, C. C., Larsen, E., Fractal Geometry of Two-Dimensional Fracture Networks at Yucca Mountain, Southwestern Nevada, Office of Scientific & Technical Information Technical Reports, US Department of Energy, OSTI, Ouk Ridge, Tenn., USA, 1985
[15] Stauffer, D., Introduction to Percolation Theory, *Physics Today*, *46* (1993), 40, pp. 64-64
[16] Masihi M., *et al.*, Fast Estimation of Connectivity in Fractured Reservoirs Using Percolation Theory, *SPE Journal*, *12* (2007), 02, pp. 167-178
[17] Balberg I., *et al.*, Excluded Volume and Its Relation to the Onset of Percolation, *Physical Review B*, *30* (1984), 7, pp. 3933-3943

Paper submitted: March 10, 2017
Paper revised: May 1, 2017
Paper accepted: May 21, 2017